Polar Oxide Interface Stabilization by Formation of Metallic Nanocrystals

Vlado K. Lazarov,[1] Scott A. Chambers,[2] and Marija Gajdardziska-Josifovska[1]

[1]*Department of Physics and Laboratory for Surface Studies, University of Wisconsin–Milwaukee, Milwaukee, Wisconsin 53211, USA*

[2]*Fundamental Science Division, Pacific Northwest National Laboratory, Richland, Washington 99352, USA*

(Received 22 November 2002; published 30 May 2003)

In situ x-ray photoelectron spectroscopy and *ex situ* transmission electron microscopy and diffraction studies of a model $Fe_3O_4(111)/MgO(111)$ polar oxide interface exclude stabilization by interface faceting, reconstruction, or by formation of a continuous interfacial layer with altered stoichiometry, and uncover stabilization by dominant formation of metallic Fe(110) nanocrystals. The iron nanocrystals nucleate both at the interface and within the magnetite film and grow in a Nishiyama-Wasserman orientation relationship with a bimodal size distribution related to twinning. Minority magnetite nanocrystals were also observed, growing in the less polar (100) orientation than the magnetite (111) film. Electron transfer and bond hybridization mechanisms are likely at the metal/oxide and oxide/oxide interfaces and remain to be explored.

DOI: 10.1103/PhysRevLett.90.216108 PACS numbers: 68.47.Gh, 61.14.Lj, 68.37.Lp, 68.55.Jk

The ionic character of bonding in metal oxides significantly affects the energetics of their surfaces. Polar oxide surfaces, classified as type III oxide surfaces [1], have a net surface charge and an electric dipole moment in the repeat unit perpendicular to the surface, causing a divergent surface energy for bulk terminated surfaces. MgO(111) (i.e., periclase) and $Fe_3O_4(111)$ (i.e., magnetite) surfaces, representative of rocksalt and inverse spinel cubic structures, have been studied as model polar oxide surfaces in the search for stabilization mechanisms that remove their diverging energy. The initially accepted model of MgO(111) faceting into neutral MgO{100} surfaces [2] is now superseded by models of MgO(111) surface reconstructions [3], surface metallization [4], and hydrogen adsorption [4,5]. A large surface relaxation has been found to stabilize the $Fe_3O_4(111)$-(1×1) surface [6].

The present experimental study extends the polar surface problem to a polar interface problem, by investigating how the polarity of an oxide substrate affects the growth of polar oxide films. Single crystals of MgO, cut on the (111) plane, were selected as model polar substrates. Fe_3O_4 has a unit cell that is almost double that of the MgO cell, with a mismatch of $\sim$0.33%. Controlled growth of magnetite films has been a subject of intense studies inspired by its many technological applications (e.g., review by Chambers and references therein [7]). This work uses heteroepitaxial growth to form a model $Fe_3O_4(111)/MgO(111)$ polar oxide interface and focuses on exploration of interface stabilization mechanisms via structural characterization. The results are benchmarked against the $Fe_3O_4(111)/Pt(111)$ polar/metal system [6] and the $Fe_3O_4(100)/MgO(100)$ polar/neutral oxide system [8].

Magnetite films were grown in an oxygen plasma-assisted molecular beam epitaxy system [7] on MgO(111) single crystals cleaned by *in situ* oxygen plasma etching and 800 °C electron-beam annealing. The substrate was held at 250 °C during growth. Fe was evaporated from an electron-beam evaporator at constant flux of 0.6 Å in an activated oxygen beam characterized by a pressure of 1.0×10^{-5} Torr measured outside the beam and a power level of 200 W within the electron cyclotron resonance plasma module. These conditions were previously optimized for epitaxial growth of single-phase $Fe_3O_4(100)$ films on MgO(100) substrates [8]. Two growth experiments were performed under the same conditions but with varying deposition times, producing films with nominal thicknesses of 80 and 250 nm. The films were characterized *in situ* by reflection high-energy electron diffraction (RHEED) and x-ray photoelectron spectroscopy (XPS). Further *ex situ* transmission electron microscopy (TEM) characterization included bright field (BF) and dark field imaging, high-resolution transmission electron microscopy (HRTEM), selected area diffraction (SAD), and convergent beam electron diffraction (CBED), performed with a Hitachi H-9000 NAR microscope operated at 300 keV. Cross-section specimens in $[1\bar{1}0]$ and $[11\bar{2}]$ zones and plan view [111] zone specimens were prepared with standard TEM methods.

RHEED was used to monitor the growth of the films, indicating that the first several monolayers grow predominantly as well ordered magnetite epitaxial layers. Additional nonspinel reflections developed concurrently, suggesting the nucleation of secondary phases within the magnetite film. The magnetite RHEED pattern gradually faded as the growth proceeded, developing into polycrystalline ring patterns superimposed on a very weak spinel-like single-crystal pattern. *In situ* XPS from the as-grown films [Fig. 1(a)] revealed a surprising presence of Fe^0, in addition to the Fe^{2+} and Fe^{3+} peaks that were expected for Fe_3O_4. Elemental iron was not observed in XPS

spectra from $Fe_3O_4(100)$ films grown on the neutral MgO(100) surface under the same conditions [Fig. 1(b)]. Single-phase $Fe_3O_4(111)$ films have also been grown by oxidation on Fe(110) crystals [10] and by successive oxidation of Fe monolayers on Pt(111) substrate [6] under similar conditions. While the Fe^0 peaks in Fig. 1(a) are unique identifiers of a metallic phase in the iron oxide film, a question remained whether there are other oxides present in addition to magnetite. The Fe^{2+} peak can also be indicative of FeO (wustite), while Fe^{3+} can be indicative of both the cubic and hexagonal phases of Fe_2O_3 (maghemite and hematite). The chemical shifts of the oxygen peak are too small to allow the determination of iron oxide phases from XPS. Hence, we undertook electron microscopy and diffraction characterization of the films.

Cross section BF-TEM reveals an abrupt and flat film/MgO(111) interface without any signs of interface faceting into neutral MgO{100} faces [Figs. 2(a) and 2(b)]. Backed by HRTEM observations (e.g., Fig. 3), these experiments rule out interface micro- and nanofaceting as possible stabilization mechanisms for this polar oxide interface system. The film surface in Fig. 2(a) displays flat and faceted regions, but this surface morphology appears correlated with the presence of inclusions in the film.

The denser inclusions become particularly visible with a darker contrast when the MgO substrate (light gray) and the epitaxial magnetite film (gray) are tilted away from a zone axis to a weakly diffracting orientation, as in Figs. 2(b) and 2(c). These dark inclusions have a bimodal size distribution. The dominant smaller inclusions are elongated along the three equivalent $\langle 1\bar{1}0\rangle$ directions of the MgO substrate having average projected lengths of 75 ± 20 nm and average projected widths of 43 ± 9 nm as measured from plan view images. The cross-section images reveal that most of the small inclusions nucleate at the MgO(111) surface and within the first few monolayers of the magnetite film, becoming fully enveloped by the film without perturbing the $Fe_3O_4(111) \parallel MgO(111)$ epitaxial relationship (e.g., Fig. 3). Their average thickness along the growth direction is 18 ± 4 nm.

Nearly 10% of the dark inclusions are substantially larger and less elongated, having an average length of 350 ± 85 nm (approximately along the $\langle 11\bar{2}\rangle$ directions) and width of 250 ± 83 nm (approximately along the $\langle 1\bar{1}0\rangle$ directions) in plan view. When observed in cross section, some of these larger inclusions appear to nucleate at the interface as standard small inclusions, then change their habit and grow as columns to the top of the film.

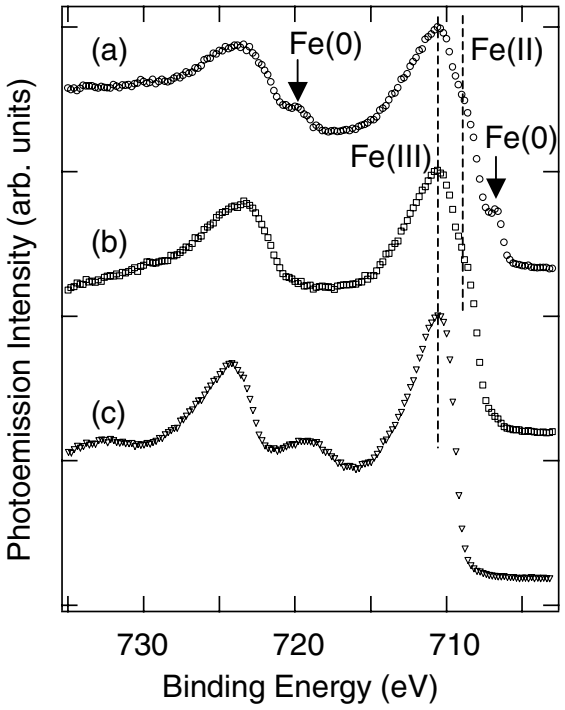

FIG. 1. *In situ* XPS of as-grown $Fe_3O_4(111)/MgO(111)$ film showing the presence of elemental iron, Fe(0), in addition to Fe(II) and Fe(III), associated with $Fe_3O_4(111)$ [curve (a)]. Also shown are reference spectra for $Fe_3O_4/MgO(001)$ [curve (b)] and γ-$Fe_2O_3/MgO(001)$ [curve (c)] grown in the same chamber (Ref. [9]).

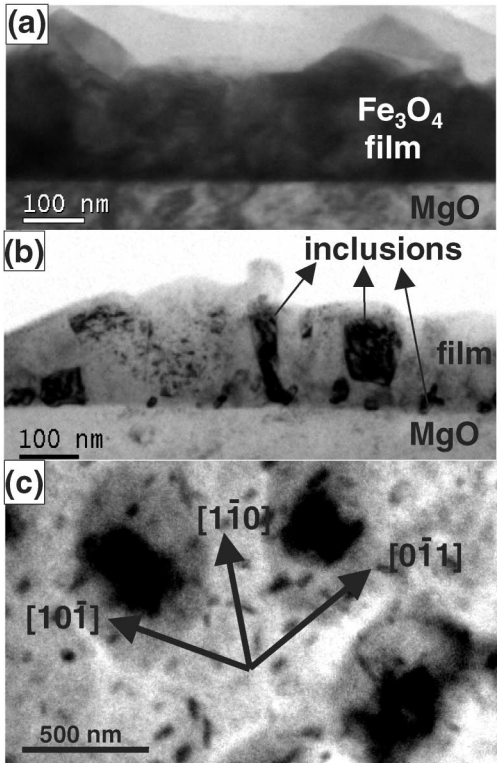

FIG. 2. BF TEM micrographs from (a) cross sectional sample in $[1\bar{1}0]$ zone showing abrupt interface and partially faceted surface; (b) cross sectional sample tilted from $[1\bar{1}0]$ zone showing inclusions with different shape and size, nucleated on the interface and within the film; (c) plane view sample tilted from [111] zone showing bimodal size distribution of inclusions and elongation in three $\langle 1\bar{1}0\rangle$ equivalent directions (smaller inclusions) and in $\langle 11\bar{2}\rangle$ directions when twinning occurs (large inclusions).

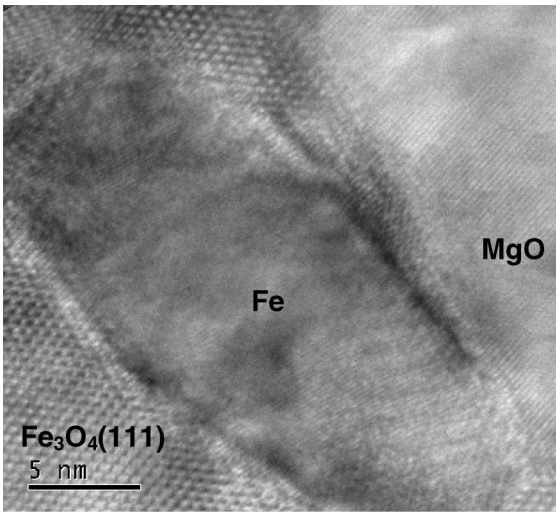

FIG. 3. HRTEM image of cross section sample showing a smaller Fe nano-inclusion nucleated on the interface and enveloped fully within the epitaxial Fe_3O_4(111) film.

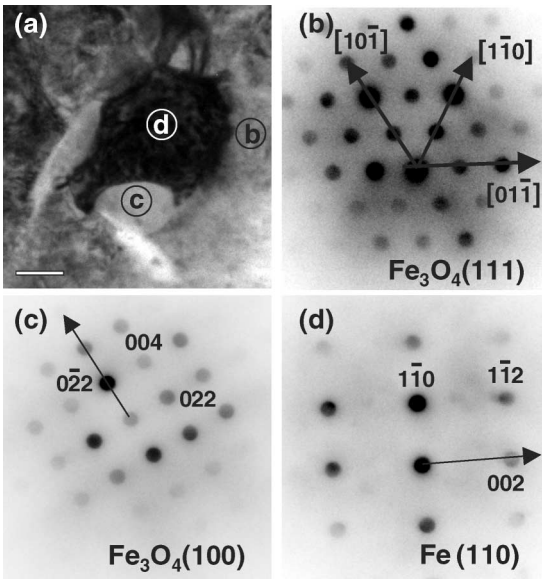

FIG. 4. Plan view BF image (a) with labeled areas from which CBED patterns (b)–(d) are obtained. (b) Fe_3O_4(111) film with outlined $\langle 1\bar{1}0\rangle$ equivalent directions. (c) Fe_3O_4(100) inclusion with $(0\bar{2}2) \parallel (10\bar{1})$ film. (d) Fe(110) inclusion with $(002) \parallel (01\bar{1})$ film.

Others appear blocklike and can nucleate close to the interface or within the film, often terminating within the film. The pronounced surface faceting of the film appears to be driven by these larger nano-inclusions.

Phase identification of the film and inclusions was obtained from numerical diffractograms of HRTEM images and from electron diffraction patterns recorded with convergent and parallel illumination (CBED and SAD). A 45 nm convergent probe was used to obtain CBED patterns, as in Fig. 4, showing the three film phases: the epitaxial Fe_3O_4 film in [111] zone, an Fe_3O_4 inclusion in [100] zone, and a large α-Fe (i.e., bcc) inclusion in [110] zone. Since these patterns were taken in plan view, the zone axis orientation of each of the phases coincided with their growth direction. Systematic CBED studies found that the majority of small inclusions and all big inclusions were elemental Fe(110), while a minority of the small inclusions were Fe_3O_4(100), which was confirmed by HRTEM and SAD data from different regions and substrate zones.

The crystallographic orientation relationship of the different phases was determined from diffraction experiments conducted in the three mutually perpendicular MgO zones: [111], $[1\bar{1}0]$, and $[11\bar{2}]$. The fcc oxygen sublattices of MgO and magnetite are essentially identical, driving the perfect heteroepitaxial match between the substrate and the dominant Fe_3O_4(111) film phase, with all equivalent axes parallel to each other. The small and large Fe grow with their (110) planes parallel to the polar surface, as reported previously in growth experiments of Fe, Nb, Mo, and Cr on MgO(111) [11]. Their in-plane orientation obeys the Nishiyama-Wasserman (NW) bcc-fcc orientation relationship where $(110)\text{bcc} \parallel (111)\text{fcc}$, $(001)\text{bcc} \parallel (1\bar{1}0)\text{fcc}$, and $(1\bar{1}0)\text{bcc} \parallel (11\bar{2})\text{fcc}$. There are three equivalent $\langle 1\bar{1}0\rangle$ directions on the fcc (111) surface, resulting in three rotationally related Fe(110) domains. For example, the CBED pattern in Fig. 4(d) shows one NW domain where the (002) Fe reflection closely matches the MgO $(02\bar{2})$ and the Fe_3O_4 $(04\bar{4})$ reflections. This one-directional match explains the pronounced elongated shape of the smaller single-crystal Fe inclusions along the three equivalent $\langle 1\bar{1}0\rangle$ directions [e.g., Fig. 2(c)]. The small Fe nanocrystals were found to be free of twins, while many of the large Fe nanocrystals displayed twinning on the $\{11\bar{2}\}$ planes, resulting in three additional Fe(110) domains and causing the observed rotation of their elongation towards the three equivalent $\langle 11\bar{2}\rangle$ directions. Twinning is a possible mechanism that explains how some of the small inclusions can release the stress from the partial epitaxy and promote the growth of bigger Fe inclusions. Multidomain growth with twinning in a Kurdjumov-Sachs (KS) orientation relationship was recently found for Mn(110) on MgO(111) [12]. The KS, Bain, and Homma-Yang-Schuller bcc-fcc relationships were also explored as possible sources of the bimodal Fe size distribution, but were not found to match our data.

The minority phase Fe_3O_4(100) inclusions were found to share {110} type planes with the magnetite (111) film or closely match their {026} type planes to the Fe {002} planes. Further details of their orientation relationships will be reported elsewhere. Here we note that degeneracy of the 15 possible rotational domains resulted in six unique orientations, accounting for the ringlike spinel RHEED patterns that were observed in the *in situ* experiments. FeO and Fe_2O_3 were not found at the interface or within the magnetite film.

In the absence of theoretical predictions for instability of polar oxide interfaces, or for their stabilization

mechanisms, we use analogy with polar oxide surfaces to initiate the discussion. Our data eliminate interface faceting and interface reconstruction as possible stabilization mechanisms and exclude interface metallization by formation of a continuous metal layer in between the polar oxide substrate and the polar oxide film. A continuous iron oxide interface layer with different stoichiometry and polarity was also not seen. Instead, a nanodot variant of the last two options was found, via phase separation that occurs during growth of magnetite (111) polar films on MgO(111) polar substrates, resulting in creation of majority Fe(110) and minority magnetite(100) nanocrystal inclusions. Such phase separation does not occur when polar magnetite films are grown on metal substrates [6,10] and on neutral oxide substrates [8], suggesting that the substrate polarity is the dominant cause for the observed phase separation in the polar oxide film. Electron transfer and/or bond hybridization at a metal/polar-oxide interface have also been proposed as mechanisms for substrate polarity reduction, as in the *ab initio* theoretical studies of several transition metals on MgO(111) [13,14] and the experimental study of Cu/MgO(111) [15]. The predicted metal polarization and enhanced adhesion [13] that result from the electron transfer mechanisms could also drive the formation of the Fe/MgO(111) and the Fe/Fe_3O_4(111) interfaces in our system, but our structural data are not suitable for direct verification of electronic mechanisms. Similarly, we cannot say if electron transfer provides a concurrent stabilization mechanism for the Fe_3O_4/MgO(111) interface regions.

The minority magnetite (100) inclusions appear to be a less favorable solution to the polarity problem than the Fe inclusions. Their presence within the magnetite (111) film can be rationalized from their lesser polarity (Table I) and because some of these polar magnetite (100) inclusions can nucleate on the metal Fe inclusions. The lattice mismatch of both inclusion phases with the MgO substrate and the magnetite (111) film is the most likely cause for their nanoscale dimensions, but the substrate polarity and the magnetic nature of the film and inclusions may also play a role in constraining their growth.

While it is too early to predict with any certainty if the discovered metal nanocrystal mechanism will be general for all polar oxide interfaces, it is reasonable to expect that phase separation would be dominant in other highly polar systems, while electron transfer or interface reconstruction mechanisms (without phase separation) would be likely for less polar interfaces. A recent, yet unpublished, study by Farrow *et al.* has found a similar phase separation when magnetite (111) is grown on sapphire (0001), reporting large effects on the magnetic properties relevant for magnetic tunneling junctions [16].

In summary, the MgO(111) surface polarity significantly influences the structure of epitaxially grown Fe_3O_4(111) polar film by inducing growth of Fe(110) and Fe_3O_4(100) nano-inclusions at both the interface and within the film. The major phase is elemental Fe, which appears to offer a solution to the polarity of the substrate and the film. Our findings suggest that surface and interface polarity can provide a novel growth mechanism for metal nanocrystals within oxide films.

TABLE I. Electric dipole moment normal to MgO(111), Fe_3O_4(100), and Fe_3O_4(111) bulk terminated surfaces, calculated in Debye ($1\ \mathrm{D} = 3.336 \times 10^{-30}$ C m) per unit area and volume using their bulk interlayer spacings and ionic charges. MgO(111) and Fe_3O_4(100) values are independent of stacking; $3Fe_B/4O/Fe_A/Fe_B/Fe_A/4O$ stacking is used for Fe_3O_4(111) value, with tetrahedral and octahedral position of Fe denoted as *A* and *B*, respectively.

	μ/A (D/Å^2)	μ/V (D/Å^3)
MgO(111)	1.52	0.62
Fe_3O_4(100)	0.42	0.25
Fe_3O_4(111)	3.40	0.69

This study was sponsored by a National Science Foundation Presidential Faculty fund (NSF/DMR–9553148). The film growth and *in situ* characterization were performed in the Environmental Molecular Sciences Laboratory, a national scientific user facility sponsored by the Department of Energy's Office of Biological and Environmental Research and located at Pacific Northwest National Laboratory. We thank D. Robertson for assistance with TEM specimen preparation.

[1] P.W. Tasker, J. Phys. C **12**, 4977 (1979).
[2] V. E. Henrich, Surf. Sci. **57**, 385 (1976).
[3] R. Plass *et al.*, Phys. Rev. Lett. **81**, 4891 (1998).
[4] A. Pojani, F. Finocchi, J. Goniakowski, and C. Noguera, Surf. Sci. **387**, 354 (1997).
[5] K. Refson *et al.*, Phys. Rev. B **52**, 10 823 (1995).
[6] W. Weis, A. Barbieri, M. A. VanHove, and G. A. Samorjai, Phys. Rev. Lett. **71**, 1848 (1993).
[7] S. A. Chambers, Surf. Sci. Rep. **39**, 105 (2000).
[8] S. A. Chambers, S. Thevuthasan, and S. Joyce, Surf. Sci. **450**, L273 (2000); B. Stanka, W. Hebenstreit, U. Diebold, and S. A. Chambers, *ibid.* **448**, 49 (2000).
[9] S. A. Chambers and S. A. Joyce, Surf. Sci. **420**, 111 (1999).
[10] V. S. Smetenkowski and J. T. Yates, Surf. Sci. **232**, 113 (1990).
[11] J. E. Mattson, E. E. Fullerton, C. H Sowers, and S. D. Bader, J. Vac. Sci. Technol. A **13**, 276 (1995).
[12] I. L. Grigorov, M. R. Fitzsmmons, I-Liang Siu, and J. C. Walker, Phys. Rev. Lett. **82**, 5309 (1999).
[13] J. Goniakowski and C. Noguera, Phys. Rev. B **60**, 16 120 (1999); **66**, 085417 (2002).
[14] R. Benedek, M. Minkoff, and L. H. Yang, Phys. Rev. B **54**, 7697 (1996).
[15] D. A. Muller *et al.*, Phys. Rev. Lett. **80**, 4741 (1998).
[16] R. F. C. Farrow *et al.*, J. Appl. Phys. (to be published).